Integrating Point Spread Function Into Taxel-Based Tactile Pattern Super Resolution

Bing Wu and Qian Liu

Abstract—**The past decade has witnessed the development of tactile sensors, which have been increasingly considered as an essential equipment in robotics, especially the dexterous manipulation and collaborative human-robot interactions. There are two major types of tactile sensors, i.e., the vision-based and taxel-based sensors. The latter is capable of achieving lower integration complexity with existing robotic systems, but unable to provide high-resolution (HR) tactile information as that of the vision-based counterpart due to the manufacturing limitations. Therefore, we propose a novel tactile pattern super-resolution (SR) scheme for taxel-based sensors, which is a data-driven scheme enabling customized selection on the number of applied "tapping" actions to achieve improvable performance from single tapping SR (STSR) to the multi-tapping SR (MTSR). In addition, we develop a new dataset for the proposed tactile SR scheme. In order to obtain scalable resolutions (e.g. $\times 4$, $\times 10$, $\times 20$, etc.) of ground-truth HR tactile patterns, we propose a novel tactile point spread function (PSF) scheme to generate HR tactile patterns by leveraging the low-resolution (LR) data gathered directly from the taxel-based sensor and the depth information of contact surfaces. This is in strong contrast to the conventional ground-truth generation approach with overlapped multi-sampling and registration strategy, which can only provide a fixed resolution. Experimental results confirm the efficiency of the proposed scheme.**

Index Terms—**Tactile super resolution, tactile perception, tactile PSF.**

I. Introduction

The tactile sensing plays an important role in human perceptions, which allows us to engage with the surrounding environments and obtain valuable touch feedback on the properties of objects and surfaces. With the continuous advancement of robotics and augmented/virtual reality technologies, there is an increasing demand for tactile sensors that can replicate the rich and delicate perception of human touch. High-resolution (HR) tactile data can enhance the ability of robots to execute intricate manipulation tasks [1], as well as improving the user's experience during human-robot interactions [2].

Manuscript received 20 April 2023; revised 22 November 2023 and 1 February 2024; accepted 17 February 2024. Date of publication 28 February 2024; date of current version 19 December 2024. This work was supported in part by the National Science Foundation of China under Grant 62071083, and in part by the Dalian Science and Technology Innovation Foundation under Grant 2022JJ12GX014. This paper was recommended for publication by Associate Editor H. Kajimoto and Editor-in-Chief D. Prattichizzo upon evaluation of the reviewers' comments. *(Corresponding author: Qian Liu.)*

The authors are with the Department of Computer Science and Technology, Dalian University of Technology, Dalian 116024, China (e-mail: wb1595946882@mail.dlut.edu.cn; qianliu@dlut.edu.cn).

Digital Object Identifier 10.1109/TOH.2024.3371092

Tactile signals are typically described in three categories: the force signal, the vibration signal, and the tactile pattern. The tactile pattern can capture sophisticated tactile details such as the surface texture and the contact object shape via distributed tactile sensing arrays. In this paper, the tactile pattern can be considered of as an array of data collected by the sensor, representing the deformation distribution on the sensor surface. Because of the similarity between the tactile pattern and the image, some researchers have treated it directly as an image [3], [4]. However, it is still a challenging task to obtain HR tactile pattern due to the physically low resolution (LR) of the tactile sensing hardware [5].

Over the past decade, numerous sensors have been developed to obtain HR tactile data. The highest resolution is achieved by vision-based tactile sensors [6], [7], [8], some of which can provide resolutions as fine as 1 micrometer and detect the tactile texture information at the fingerprint level. These sensors rely on a camera mounted behind a gel to capture its deformation upon contact. The captured signal is then used as the tactile pattern. Nonetheless, a tight integration of vision-based sensors to the existing systems still needs further investigation due to the critical space required by the imaging equipment. Therefore recent researches on vision-based sensors start to figure out how to reduce the size of the entire sensor (including the filming equipment) [9], [10] while increasing the sensing scale [11].

The taxel-based tactile sensor is another type of tactile sensors that operates on various physical principles such as capacitive, piezoresistive, and magnetic [12]. These sensors comprise an array of small sensing elements, called taxels. Each taxel can collect the one- or three-axis force or deformation information in a specific contact area. This type of sensor is available in various sizes and of ease to integrate into existing systems.However, most taxel-based sensors can only collect LR tactile data. Due to the current limitations in manufacturing and other factors, the resolution of advanced taxel-based sensors is $\sim$1 mm [13], [14], which is significantly lower than that of vision-based sensor. In order to improve the resolution of the tactile sensor, [13], [15], [16] have attempted to increase the sensor density. The Silicon micro-electro-mechanical system technology is used to enhance the spatial resolution [17], [18]. However, various issues emerge with the increase of the taxel density such as more wire connections, longer data acquisition time, and amplified cross-talk between taxels [19].

Therefore, tactile SR algorithms were developed aiming at predicting the HR tactile signals from physically LR taxel-based sensor array. Unlike existing algorithms, which typically focus on improving the localization accuracy of a single contact point in the taxel-based sensor, our previous work [20] is to investigate the applicability of SR methods from computer vision to the tactile field, and propose two deep learning based tactile pattern SR algorithms by adapting image SR algorithms (e.g. SRCNN [21] and SRGAN [22]). The developed schemes can achieve $\times 10$ (from 4×4 to 40×40) resolution enhancement with a single tapping of a LR taxel-based sensor. However, we further discover that the performance of these models is restricted by the resolution of ground-truth tactile patterns. In [20], LR tactile patterns cannot be predicted accurately via the down-sampling strategy, since two visually alike tactile patterns may significantly drift apart from each other with respect to the actual contact force. This leads to the method of generating HR data in [20] cannot obtain flexible scales in-between 4×4 and 40×40. Moreover, the generated HR data depends on the positioning accuracy of the robot arm, which presents challenges in obtaining HR data as ground truth at higher scaling factor. Notably, at a scaling factor of $\times 10$, the movement stepsize of the robot arm was 0.047 mm, approximating the limits of the arm's positioning accuracy. In order to overcome these problems, we propose in this paper a tactile novel point spread function (PSF) based model which helps to quickly generate high-quality HR tactile patterns with different scaling factors (e.g. $\times 4$, $\times 6$, $\times 8$, $\times 10$, and $\times 20$). The PSF can model the response of a system to a single stimulus. In the field of tactile sensing, the PSF can be used to approximate the deformation experienced during the contact process. This way, the contact pattern can be considered as the superposition of multiple point stimuli. This method offers greater efficiency compared to the multi-sampling and registration strategy [20]. This way, we build up a new dataset for the tactile SR with pairs of LR sensor data and scalable HR tactile patterns. We believe that the new dataset can be considered as a valuable reference to the future research of tactile SR.

In this paper, we tackle the challenge of SR for tactile patterns with regional or multiple contacts, and propose a data-driven tactile pattern SR scheme specifically tailored for 3-axis taxel-based sensors, which allows a customized selection of single or multiple LR inputs. All experiments are conducted with a commercial Xela tactile sensor [23], which comprises 4×4 sensing units with an 4.7 mm inter-unit spacing. The overall effective sensing area is $\sim 20\times20$ mm^2. To facilitate interaction between the tactile sensor and the contact surface, we mount the Xela tactile sensor at the end-effector of a robot arm. We only use the 3D deformation distribution information measured by the sensor, which means that the proposed scheme does not rely on any specific characteristics of sensors. Therefore, the proposed SR scheme can be directly applied to obtain HR tactile patterns with similar 3-axis taxel-based sensors without complicated adjustments. The description of abbreviation in this paper as shown in Table I.

The rest of this paper is organized as follows. Section II provides a brief literature review on the image SR, the tactile SR and the tactile sensor simulation algorithms. Section III presents the mathematical model of tactile pattern SR. Before demonstrating the proposed tactile SR scheme in Section V, we first present how to build a new dataset for the proposed research, as well as a novel tactile PSF model which is utilized to generate flexible scales of ground-truth tactile patterns in the new dataset. In Section V, we illustrate a data-driven tactile pattern SR scheme that allows a customized selection of the number of "tapping" actions. A satisfactory performance can be achieved by single tapping, which is further enhanced once adopting multi-tapping inputs collected from the LR tactile sensor array. Section VI reports the experimental results dataset related cases, as well as real-world cases. Finally, Section VII concludes the paper with a summary.

TABLE I
DESCRIPTION OF ABBREVIATIONS

Abbreviation	Definition
LR	Low Resolution
HR	High Resolution
SR	Super Resolution
PSF	Point Spread Function
STSR	Single Tapping Super Resolution
MTSR	Multi-Tapping Super Resolution
PSNR	Peak Signal-to-Noise Ratio
SSIM	Structural SIMilarity

II. Related Work

A. Image SR

Image SR algorithms have been extensively studied in the field of computer vision [24]. In the case of single image super-resolution, an HR image is generated from a single LR image via an SR model, which generally employs the prior knowledge of the LR image or the dataset for predication. The famous SRCNN [21] and SRGAN [22] models belong to the category of Single Image Super-Resolution. On the other hand, the multi-image or video super-resolution approaches reconstruct an HR image from multiple LR frames, incorporating not only the prior knowledge of the current frame but also that of adjacent frames. A notable example of the video super-resolution algorithm is the VSRnet [25].

B. Tactile SR

Existing researches on the tactile SR basically focus on locating an HR contact point when a single stimulus is applied to the LR tactile sensor, which can be referred as the localization SR [26]. Bayesian active perception algorithms were proposed in [26], [27] to classify contact surfaces on taxel-based and vision-based sensors, respectively, which achieved 35-fold and 40-fold improvements in the localization accuracy. A data-driven approach was presented in [28] using multiple Takktile pressure sensors in the shape of a dome, which obtained a nearly 15-fold improvement in the localization accuracy. The Taxel Value Isolines model was proposed in [29] to describe the tactile localization SR process and achieved a 109-fold improvement in the 1-D scenario and a 1254-fold in the 2-D case. The Local Message Passing Network in [30], calibrated sensor arrays using single-touch data for multi-touch scenarios. However, sensors used in the above studies only measured the Z-axis deformation or force signal during the contact process, neglecting the shear signal. In contrast, [31] presented a 3-axis magnetic tactile skin capable of detecting and interpreting force and location data in real-time. [32] used a 3-axis tactile sensor to achieve a 60-fold improvement in the localization accuracy and quantitatively described the role of the shear force in the SR process. [33] utilized the sensor-specific properties to obtain the single-point and multi-point tactile localization SR for a single taxel. All of these approaches were proposed to improve the localization resolution, and most of them are only developed for single-point contact scenarios, not applicable to the tactile pattern SR.

For Electrical-Impedance-Tomography based sensors, the contact pattern was determined by measuring the changes in current flow and the associated voltage of a ring of electrodes placed around a pressure-sensitive conductive fabric. Its spatial resolution can be improved by using a grid of internal array electrodes [34]. Deep neural networks were adopted to improve the quality of reconstructed tactile pattern [35], [36], [37].

C. Tactile Sensor Simulation

In this research, we employ the tactile sensor simulation method to generate the ground truth of different scales of HR tactile patterns in the dataset, which is achieved by simulating the deformation of the tactile sensor surface when having contacts with an object. Since most tactile sensors utilize soft materials as the sensor surface, the tactile information can be simulated as the deformation or force of an elastomer. In this context, physical simulation algorithms, such as the mass-spring model [38], [39], the finite element method [40], [41], [42], and the material point method [43], [44], can achieve this goal but with considerably high computational complexity.

Recently, data-driven methods have been introduced to the field of tactile simulation. For example, [45] used the finite element method to simulate the deformation of the BioTac sensor, then translated it into an electronic signal through a generative learning framework. Other studies (such as [46], [47]) utilized computer graphic techniques, such as ray-tracing models and example-based methods, to simulate the vision-based tactile sensors. A direct use of the PSF in the tactile simulation was proposed in [48], [49], which obtained a satisfactory match to the real data collected by the sensor with a fine calibration setup. However, as the resolution increases, the deviation between the simulated and real data enlarges. This is caused by the PSF blurring effect which will be discussed in detail in Section IV. This motivates the study on the proposed tactile PSF in this research.

III. Problem Statement

In this section, we present the mathematical model of the tactile pattern SR. Let $[\mathbf{T}_0, \mathbf{T}_1, \ldots, \mathbf{T}_k] \in \mathbb{R}^{k\times 3\times M\times N}$ be a sequence of tactile data sampled during a single contact process, where the tactile data at any time k can be decomposed into three components, i.e. $\mathbf{T}_k = [\mathbf{T}_{x,k},\ \mathbf{T}_{y,k},\ \mathbf{T}_{z,k}]$, where

$$\mathbf{T}_{x,k} = \begin{bmatrix} t_{x,k}^{0,0} & \cdots & t_{x,k}^{0,N-1} \\ \vdots & \ddots & \vdots \\ t_{x,k}^{M-1,0} & \cdots & t_{x,k}^{M-1,N-1} \end{bmatrix}_{M\times N},$$

and $t_{x,k}^{M-1,N-1}$ denotes the x-axis data of the $[M, N]$-th taxel cell at time k. We set $M = N = 4$ in this paper, which indicates that the sensor is composed of 4×4 taxels as that of the Xela tactile sensor used in this research. $\mathbf{T}_{y,k}$ and $\mathbf{T}_{z,k}$ can be obtained similarly.

The key task of tactile SR is to recover a HR tactile pattern from a LR counterpart. Similar to the image SR, we assume that the LR pattern can be considered as a degradation of the HR pattern. We define the z-axis degradation mapping function $\mathcal{D}_z$ as

$$\mathbf{T}_{z,k}^{\mathrm{LR}} = \mathcal{D}_z(\mathbf{T}_{z,k}^{\mathrm{HR}},\ \gamma_z), \tag{1}$$

where γ_z presents the set of parameters of the degradation process (e.g., the scaling factor and the noise). The above degradation function is generally unknown. Hence, the task of SR is to find a $\hat{\mathbf{T}}_k^{\mathrm{HR}}$ as similar as the real HR pattern $\mathbf{T}_k^{\mathrm{HR}}$. When giving the LR data at the current moment, the HR data can be obtained by the prediction model shown below.

$$\hat{\mathbf{T}}_{z,k}^{\mathrm{HR}} = \mathcal{F}_z\left(\mathbf{T}_{x,y,z,k}^{\mathrm{LR}}, \theta\right), \tag{2}$$

where $\mathcal{F}_z$ denotes the SR model and θ denotes the set of parameters corresponding to the model. Since the raw LR tactile data in each axis contain limited amount of information, it is difficult to recover a HR pattern from them. Therefore, in this paper, we attempt to recover HR data of the z-axis using the LR x-, y-, and z-axis data. Finally, the task of tactile pattern SR can be described as

$$\hat{\theta} = \arg\min_{\theta}\ \mathcal{L}(\hat{\mathbf{T}}_{z,k}^{\mathrm{HR}}, \mathbf{T}_{z,k}^{\mathrm{HR}})\ +\ \lambda\Phi(\theta), \tag{3}$$

where $\mathcal{L}(\hat{\mathbf{T}}_{z,k}^{\mathrm{HR}}, \mathbf{T}_{z,k}^{\mathrm{HR}})$ denotes the loss function, which measures the gap between the ground truth and the predicted HR tactile pattern. $\Phi(\theta)$ is the regularization term, and λ is the trade-off parameter.

IV. A New Dataset for Tactile Pattern SR

[1] Before demonstrating the proposed tactile SR model, we first build a new dataset of LR and HR pairs, which is essential for the model learning of the proposed scheme. In particular, we present a new tactile PSF method, which leverages the information of the LR data and the depth of the contact pattern to create the HR ground-truth tactile patterns. This approach is a significant improvement over our previous multi-sample registration based method in [20] for the ground-truth data generation. The new approach reduces the time required to obtain the HR data, and eliminates the artifact block caused by sensor-specific properties and the motion errors of the robot arm.

A. System Setups

We employ the Xela tactile sensor [23] in this research. It is a commercially available 3-axis tactile sensor which implements the Hall effect and consists of 4×4 taxel units. We mount the Xela tactile sensor on the end effector of the Aubo-i10 robot arm from AUBO Robotics as shown in Fig. 1, which boasts a precision

[1] The tactile SR dataset is available at https://github.com/wmtlab/tactileSR.

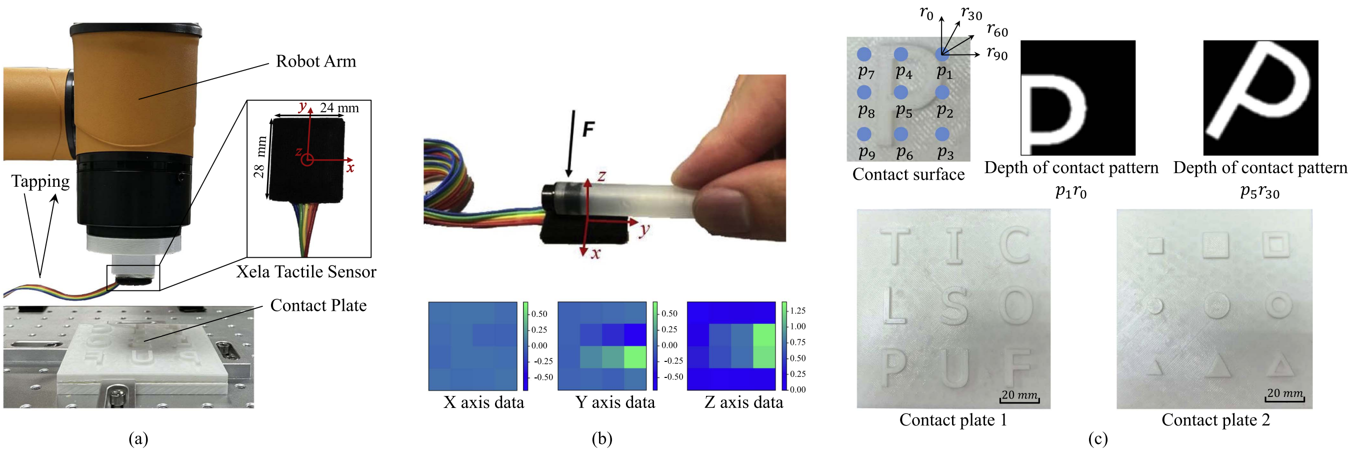

Fig. 1. Building a new dataset for the tactile pattern SR. (a) System setup: An Xela tactile sensor is attached to the Aubo-i10 robot arm. LR-HR pairs are collected by tapping, which can also be described as indenting, the contact surface with the tactile sensor. (b) An example of 3-axis LR tactile pattern: Tactile signals collected by the Xela tactile sensor have three axes: Z-axis tactile data indicating the positive deformation, and X- and Y-axis data indicating the corresponding shear deformation. Positive and negative signs are used to distinguish the direction of the deformation. (c) Dataset: The dataset used in this study contains 18 contact surfaces from two contact plates. Each contact surface has 36 different poses, corresponding to 36 different contact patterns, with 9 different positions and 4 different orientations. The depth image in the dataset are used to generate the ground truth deformation distribution. The variable $p_1 \sim p_9$ indicates the sensor's center position during the tapping action, and $r_0 \sim r_{90}$ indicates the sensor's z-axis orientation.

of ± 0.03 millimeters. Each taxel of the sensor is capable of capturing the 3D deformation information of a specific region and separating it into x-, y-, and z-axis signals. The z-axis signal represents the positive pressure applied to the sensor, while the x- and y-axis signals denote the shear deformation along the x- and y-axis, respectively. The sensor's maximum normal and shear force capabilities are 18 N and 5 N, respectively.

The Xela tactile sensor detects magnetic field changes in its elastic layer caused by magnetic particles, serving as the tactile signal. As the sensor's readings are influenced by surrounding magnetic field changes, a complex calibration algorithm is essential for its calibration. However, for the scope of our research, exact force values are not crucial. Therefore, we directly utilize the sensor's output values, which reflect relative force magnitudes.The sensor data and the applied force correspond to each other. The mapping between them can be found in Figs. 7 and 8 in [23].

B. LR Tactile Data Collection

We build two 3D-printed contact plates for the LR tactile data collection, each with 9 distinct contact surfaces, as shown in Fig. 1(c). The size of each contact surface is 20 mm $\times$ 20 mm, which is similar in size to the Xela tactile sensor. Contact surfaces of the first plate are regular alphabets, while the second one consists of polygons of different sizes. These contact surfaces contain tactile features of straight and curved lines, which are commonly encountered in robotic manipulation tasks.

LR data of the contact pattern are collected for the 9 different contact surfaces in 36 distinct poses. These poses consist of 9 positions, each with 4 different orientations. The data collection procedure is as follows. The robot arm is first moved directly to the given position, with the Z-axis of the tactile sensor perpendicular to the contact surface and the X-axis aligned with the given orientation. The arm then moves down slowly toward the object until the contact force reaches a specified threshold. This LR tactile data acquisition process procedure is then repeated for all designed poses. The robot arm coordinate system and the contact surface coordinate system are calibrated, allowing us to determine the depth of the contact surface by combining the posture of the end of the robot arm and the 3D model of the contact plate at the current contact moment. So far, we obtain the LR tactile data and the corresponding depth information for the new dataset. In the next section, we will illustrate how to use the proposed tactile PSF model to generate the HR ground truth tactile patterns.

It should be noted that, in this paper, we consider the contact force as the resultant force applied to the sensor along the Z-axis during the tapping process. Furthermore, the sum of the Z-axis sensor reading is employed to represent the magnitude of the contact force.

C. Proposed Tactile PSF Model

Previous work [48] have utilized the PSF to simulate LR tactile sensors. The PSF is also used to capture the effects of deformation [49], [50], [51]. In this paper, we develop a data-driven tactile PSF model to obtain the ground truth of HR tactile patterns by leveraging the LR tactile data, the corresponding depth information and the classic PSF. The use of PSF enables a rapid simulation of HR data, avoiding time-consuming procedures in the finite element method, material point method, and other physics-based simulators. In this paper, we adopt the Gaussian PSF

$$\mathrm{PSF}(m,n,F_{u,v}) = \alpha(F_{u,v}) \cdot \exp\left\{-\frac{\sqrt{(m-u)^2+(n-v)^2}}{\beta(F_{u,v})}\right\}, \tag{4}$$

which denotes the intensity subjected to the point (m,n) when the point (u,v) is stimulated by the applied force of $F_{u,v}$.

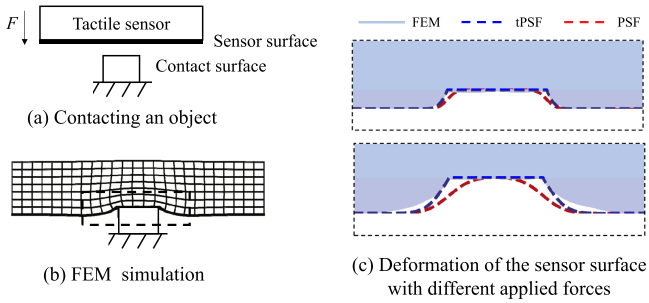

Fig. 2. Illustration of the contact procedure. (a) The tactile sensor is moving toward the object, with a constant downward force applied, assuming that the contact object does not undergo deformation. (b) The simulation of the elastic deformation of the surface with linear elastic FEM. (c) The figure above illustrates the case of a small contact force, where the tPSF and PSF predictions are similar to that of FEM with a small value of β. The figure below illustrates that the increase of the contact force leads to a larger β, and thus a larger PSF blur effect, as well as a larger difference between the PSF and FEM predictions.

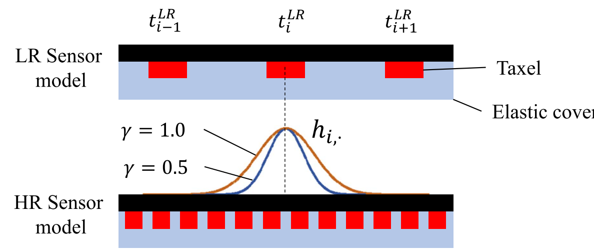

Fig. 3. Illustration of the degradation process for the HR to LR tactile pattern. The LR sensor model represents a real-world sensor with taxels placed behind an elastic medium. Upon contact with an object, the elastic medium deforms and the taxel measures the deformation of the elastomer as the tactile information. The HR sensor model is an idealized HR sensor model with smaller taxel size and smaller distances between adjacent taxels. The parameter $h_{i,\cdot}$ in this model represents the weight of the HR taxel on t_i^{LR} in the LR sensor during the degradation process.

The term $\alpha(F_{u,v})$ describes the intensity of the single point stimulus, while $\beta(F_{u,v})$ indicates the effect of this intensity on the surrounding taxel. α and β are intrinsic properties of the tactile sensor, which depend mainly on the properties of the taxel, the distribution of taxels, and the material of the sensor surface. When the sensor is given, the relationship between $\alpha(F)$ and $\beta(F)$ is determined.

For the multi-point contact or a contact pattern, it can be regarded as the superposition of a number of point stimuli, i.e., the convolution of the depth of the contact pattern and the PSF. From Fig. 6, we can see that the depth of the contact pattern and the PSF are convolved to obtain the HR tactile pattern. As the contact force increases, both α and β values of the PSF increase, resulting in a corresponding increase in the deformation of the HR tactile pattern.

Hence, we have

$$\begin{aligned}\mathbf{T}_z^{\text{HR}} &= k_{\text{scale}}\{\mathbf{I}^{\text{Depth}} * \text{PSF}(F)\}\\ t_z^{m,n} &= k_{\text{scale}} \iint \{I_{u,v}^{\text{Depth}}\text{PSF}(m,n,F_{u,v})\}\mathrm{d}u\mathrm{d}v,\end{aligned} \tag{5}$$

where $\mathbf{T}_z^{\text{HR}}$ represents the Z-axis HR tactile pattern and $t_z^{m,n}$ is the tactile signal of a single taxel located at the point (m,n) in the HR tactile pattern, which is the result of the accumulated effect of all points with $\mathbf{I}^{\text{Depth}}$. F denotes the external forces acting upon the tactile sensor surface, can be considered as the aggregation of all such individual force components experienced across the entire sensor surface.Each element of $\mathbf{I}^{\text{Depth}}$, denoted as $I_{u,v}^{\text{Depth}}$, represents the depth of the contact pattern at the point (u,v), which is normalized to the range of $[0,1]$ in this study. k_{scale} is a constant factor used to match the contact deformation between the LR and HR data.

We should point out that the Gaussian PSF has a blur effect, which becomes more severe as the applied force increases. Fig. 2(c) illustrates this effect in a one-dimensional scenario. This effect will lead to a more blurred HR tactile pattern and a greater deviation from the reality. The blur effect can be reduced by restricting the range of the Gaussian kernel. Therefore, we can define the ground truth of HR tactile pattern as

$$\mathbf{T}_z^{\text{HR}} = \begin{cases}\mathbf{I}^{\text{Depth}} * \text{PSF}(F), & t_z^{m,n} \notin \mathcal{T}\\ \max(\mathbf{I}^{\text{Depth}} * \text{PSF}(F)), & t_z^{m,n} \in \mathcal{T}\end{cases}, \tag{6}$$

where $\mathcal{T}$ denotes the area of an instant contact interaction between the contact surface and the sensor, corresponding to the top region of the 3-D printed contact pattern. The operator of $*$ denotes the convolution operation.

The HR tactile pattern can be considered as the SR of LR data. Alternatively, the LR tactile pattern can be considered as a Gaussian degradation process of the HR data, where the value of each LR taxel is determined by summing up the values of the surrounding HR taxels with Gaussian weights. For descriptive purposes, we flatten $\hat{\mathbf{T}}_z^{\text{LR}} \in \mathbb{R}^{N\times N}$ and $\mathbf{T}_z^{\text{HR}} \in \mathbb{R}^{M\times M}$ into 1D representations, resulting in $\hat{\mathbf{T}}_z^{\text{LR}'} \in \mathbb{R}^{N^2\times 1}$ and $\mathbf{T}_z^{\text{HR}'} \in \mathbb{R}^{M^2\times 1}$, respectively. Hence we have

$$\begin{aligned}\mathbf{T}_z^{\text{LR}} &= \mathcal{D}_z(\mathbf{T}_z^{\text{HR}})\\ \hat{\mathbf{T}}_z^{\text{LR}'} &= \mathbf{H}\cdot\mathbf{T}_z^{\text{HR}'} + \boldsymbol{e},\end{aligned} \tag{7}$$

where $\mathbf{H}$ is the degradation matrix, and $\boldsymbol{e}$ is the sensor noise following the Gaussian distribution with zero mean and variance of $\delta\mathbf{I}$, where $\mathbf{I}$ is the identity matrix. Expanding the degradation matrix, we have

$$\begin{bmatrix} t_0^{LR}\\ \vdots \\ t_{N^2-1}^{LR}\end{bmatrix} = \begin{bmatrix} h_{0,0} & \cdots & h_{0,M^2-1}\\ \vdots & \ddots & \vdots\\ h_{N^2-1,0} & \cdots & h_{N^2-1,M^2-1}\end{bmatrix}\cdot\begin{bmatrix} t_0^{HR}\\ \vdots \\ t_{M^2-1}^{HR}\end{bmatrix} + \boldsymbol{e},$$

where the degradation matrix $\mathbf{H}$ has a dimension of $N^2 \times M^2$, and each row $h_{i,\cdot}$ describes the influence of each taxel of $\mathbf{T}_z^{\text{HR}}$ on the ith taxel of $\mathbf{T}_z^{\text{LR}}$, as shown in Fig. 3.

Thus, the effect of the ith taxel of the HR data on the jth taxel of the LR data during the degradation process can be expressed as

$$h_{i,j} = \exp\left(-\frac{\text{dis}(t_i^{LR}, t_j^{HR})}{\gamma^2}\right)\cdot\frac{1}{\max(h_{i,\cdot})}, \tag{8}$$

where $\text{dis}(t_i^{LR}, t_j^{HR})$ is the spatial distance between the two taxels. The variable γ represents each taxel's perceptual region

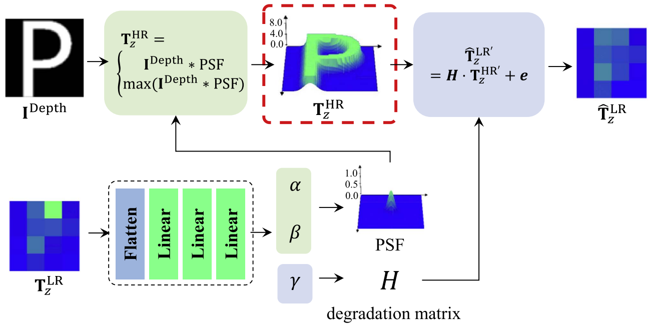

Fig. 4. Diagram of proposed tactile PSF scheme with learnable PSF and degradation parameters. The LR z-axis tactile data $\mathbf{T}_z^{\mathrm{LR}}$ is the input to three fully-connected layers to predict parameters of α, β and γ, where α and β describe the contact force at the current moment and are used in the PSF. The HR tactile data $\mathbf{T}_z^{\mathrm{HR}}$ is then obtained by convolving the depth $\mathbf{I}^{\mathrm{Depth}}$ of the contact pattern with the PSF. The third parameter γ is used to describe the degradation process.

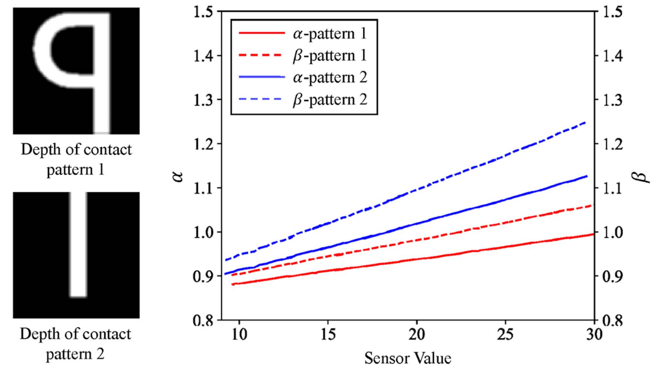

Fig. 5. Variation of PSF parameters in response to different contact patterns and forces. As the sensor value increases, or the contact force becomes larger, both α and β values for both contact patterns increase. Since *pattern1* has a larger contact area, its α and β values are smaller when the contact forces are the same.

during the degradation process. In this paper, we assume that each LR taxel experience the same degradation, resulting in the same γ for all taxels in the LR data during the degradation process.

In this paper, we propose a tactile PSF scheme to obtain the HR data with learnable PSF and degradation process parameters as shown in Fig. 4. We adopt planar contact surfaces in this research. As a result, a single PSF is used to describe the stimuli for all points in a contact pattern. The z-axis data $\mathbf{T}_z^{\mathrm{LR}}$, collected by the tactile sensor, is directly related to the applied force $F_{u,v}$, and used as the input to the model. The parameters α, β, and γ are estimated through a network with three fully-connected layers. The first two parameters, α and β, describe the PSF. The PSF is convolved with the depth to obtain a HR tactile pattern $\mathbf{T}_z^{\mathrm{HR}}$, which is used as the ground truth in the new tactile pattern SR dataset. The degradation process is uniquely determined by γ, which describes the perceptual region of each taxel in the LR sensor. The larger is γ, the larger is the perceptual area. Then, the loss function can be defined as:

$$\mathcal{L}(\hat{\mathbf{T}}_z^{\mathrm{LR}}, \mathbf{T}_z^{\mathrm{LR}}) = \left\| \mathbf{T}_z^{\mathrm{LR}} - \hat{\mathbf{T}}_z^{\mathrm{LR}} \right\|_2^2. \tag{9}$$

Therefore, the objective function of the proposed tactile PSF model is

$$< \hat{\alpha}, \hat{\beta}, \hat{\gamma} >= \arg \min_{\alpha,\beta,\gamma} \mathcal{L}(\hat{\mathbf{T}}_z^{\mathrm{LR}}, \mathbf{T}_z^{\mathrm{LR}}), \tag{10}$$

which aims at minimizing the difference between the predicted Z-axis LR data $\hat{\mathbf{T}}_z^{\mathrm{LR}}$ and that collected by the LR tactile sensor $\mathbf{T}_z^{\mathrm{LR}}$.

D. Generation of HR Tactile Patterns

The tactile PSF model is trained using the data collected in Section IV (b). Fig. 5 illustrates the variation of PSF parameters with the contact force for two different contact patterns. We observe that α and β increase linearly with the force, where α represents the increase in deformation on the individual taxel and β denotes the increase of impacts applied to the surrounding area. As the contact area of *pattern1* is larger than that of *pattern2*, the latter exhibits higher α and β under the same contact force, as shown in Fig. 5. These results are in line with intuition and demonstrate the effectiveness of the tactile PSF model.

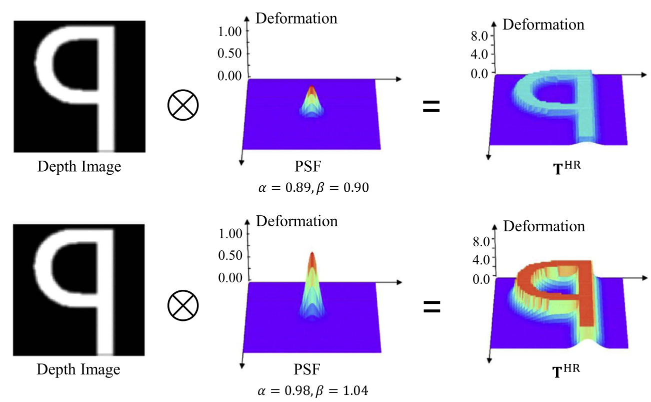

Fig. 6. Estimated PSF parameters are utilized to generate the PSF, depicting the current contact force. Then, this PSF is convolved with depth image to generate HR tactile patterns, which serve as the ground truth for tactile SR model training.

The PSF represents the current contact deformation, which is convolved with depth image to generate HR tactile patterns, as illustrated in Fig. 6. The generated HR data serve as the ground truth for training tactile SR model in Section V. We employ the Mooney-Rivlin hyperelastic model to simulate the sensor deformation, and regard the simulation result to be precise representation of the deformation distribution of the sensor surface.

We test 9 different contact surfaces on contact plate 1 at the $p_5 r_0$ position, as shown in Fig. 1(c), and compare the HR data generated by three different methods with the precise HR data obtained from FEM simulation, as depicted in Fig. 7. The results indicate that for planar surfaces, our proposed tPSF more effectively mimics the deformation distribution on the contact surface than the other two methods. Additionally, we discover that as the contact force increases, the blurring effect of the PSF

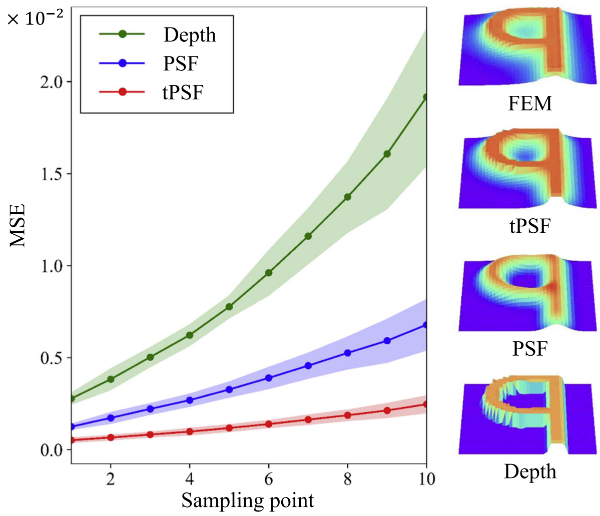

Fig. 7. Comparison between HR data generated using different methods and the FEM simulation results. The tPSF method is introduced in Section IV-C, while the PSF approach is described in [48], [49]. The 'Depth' method refers to the direct multiplication of depth with the contact force. The horizontal axis represents sampling points. To compare the generated HR data with FEM simulation results, we uniformly selected 10 sampling points from the initial contact to the maximum contact force moment.

becomes more obvious, leading to a larger deviation between the generated HR data and the FEM results. However, by restricting the convolution area, the tPSF effectively reduces the impact of Gaussian blur, thereby enhancing the model's accuracy and stability under varying contact forces.

In conclusion, we build up a new dataset for tactile SR, which contains 648 contact patterns collected with different poses of 18 contact surfaces, as shown in Fig. 11.

V. Tactile Pattern SR Model

In this section, we demonstrate the proposed tactile SR model, which is a data-driven model that allows a customized selection of single or multiple LR inputs. This is different from TactileSRCNN and TactileSRGAN proposed in [20], where only the Single-tapping SR (STSR) is performed.

The proposed tactile pattern SR scheme is illustrated in Fig. 8, which is comprised of three key modules: the input layer, the feature extraction layer, and the output layer. The input layer performs up-sampling on the LR input data to increase its dimensionality. A convolution layer is then applied to increase the number of feature channels. The feature extraction layer consists two parts, the pattern feature extraction and the force feature extraction. We use a multi-scale residual block [52] to implement the pattern feature extraction. The multi-scale residual block employs a double bypass network, which can effectively extract features at different scales and has been demonstrated to be effective in [20]. The multi-scale residual block also includes a batch normalization layer, which can improve the convergence of the network, and prevent gradient disappearance and explosion. However, since the batch normalization layer normalizes the input data, it causes a loss of the force feature. To overcome this shortcoming, we use a single residual block layer without the batch normalization layer to extract the force feature. This allows the model to converge quickly while retaining the force feature, which is distinct from the TactileSRCNN model proposed in [20]. Finally, the pattern and force feature are fused in the output layer, and the resulting pattern is resized to match the target resolution.

Since the proposed scheme allows a customized selection of "tapping" actions, we define the corresponding algorithms as Single-tapping SR (STSR) and Multi-tapping SR (MTSR), respectively. The STSR only uses the x-,y- and z-axis LR data collected at the current moment to predict the HR tactile pattern, which share the same concept of single image super-resolution task in computer vision. However, in contrast to single image super-resolution, which generally focuses on recovering both contours and textures information lost in LR images, the LR data in the tactile filed contains much less information due to the limited resolution of sensors. Therefore, we focus on recovering the contours of the contact surface rather than the more intricate texture information in this paper.

MTSR aims to predict the HR data on the contact surface using the LR sequence data collected from multiple tapping instances with different sensor poses. The tactile sensor (along with the robot arm) rotates an angle of θ_0 after the 1st tapping as shown in Fig. 10, then rotates an angle of θ_1 after the 2nd tapping, and so on, until reaches the maximum number of allowance. We assume that a total of K tappings are performed. The first $K-1$ tappings reveal the shape information of the contact pattern, while the Kth tapping is used to obtain the force features of the contact surface in addition to the shape information. To accomplish this, all K LR data acquired from all tappings are fed into the pattern feature extraction layer through up-sampling and convolution operations. The Kth LR data is then input into the force feature extraction layer, as shown in Fig. 8.

In particular, the proposed scheme can achieve satisfactory performance by using only one tapping instant i.e. $K = 1$, where both the force and pattern features are extracted from the LR tactile data collected within the single tapping process.

VI. Experimental Results

The system setup is shown in Fig. 1(a). We utilize a 4×4 taxel-based sensor to collect LR tactile data. In order to present the performance of the proposed tactile pattern SR scheme, we compare it with the conventional Bilinear interpolation algorithm, as well as the state-of-the art TactileSRCNN and TactileSRGAN developed in [20], with respect to the contact surface within the dataset and the real-world cases. In this paper, we set the maximum tapping number in the MTSR algorithm as 7, and $\theta_0 = \theta_1 = \cdots = \theta_K = 5^{\circ}$. The weights of the network are initialized with the Kaiming initialization method [53] with an Adam optimizer weight decay of 1e-2 and batch size of 8.

The depth and LR tactile patterns collected during data collection are input into the trained tactile PSF model to obtain the HR tactile pattern, which serves as the ground truth for the SR model training. The contact surface was subjected to 36 distinct contact patterns, each representing a single tapping event. For

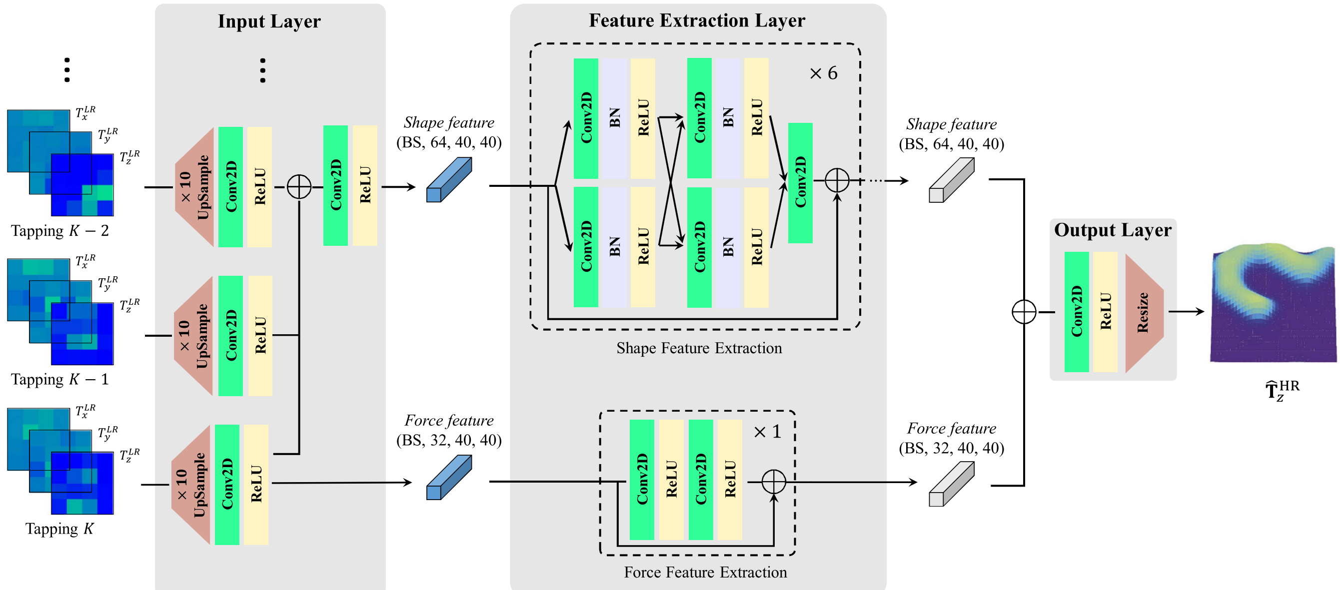

Fig. 8. Architecture of the tactile pattern SR model. The model consists of an input layer, a feature extraction layer, and an output layer. The leftmost block represents the input layer, which transforms input data of varying dimensions into fixed-dimensional variables for the feature extraction layer. The middle block is the feature extraction layer, composed of shape feature extraction and force feature extraction. The shape feature extraction extracts shape information from the input features, while the force feature extraction extracts information about the contact force. The rightmost block represents the output layer, where the pattern and force features are fused, and the output is resized to the desired resolution.

TABLE II
DATA SPLIT OF SINGLE TAPPING SR

	training	validation	testing
# of contact pattern	504	72	72
# of LR-HR pairs	8064	1152	1152

each tapping, 16 LR tactile patterns are evenly selected from the beginning of the tapping to the set contact force and used as training data. The dataset is split as shown in Table II.

A. SR Evaluation Metric

In the image SR task, two metrics, Peak Signal-to-Noise Ratio (PSNR) and Structural SIMilarity (SSIM), are commonly used to measure the difference between the SR image and the ground truth [54]. As the data formats of tactile patterns and images are similar, we also adopt these two metrics to evaluate the performance of tactile pattern SR.

1) Peak Signal-to-Noise Ratio (PSNR): It is defined by the maximum sensor value (denoted as L) and the mean squared error (MSE) between patterns. Given the ground truth of tactile pattern T with N taxels and the reconstruction $\hat{T}$, the PSNR between T and $\hat{T}$ are defined as follows:

$$\mathrm{PSNR}(T, \hat{T}) = 10 \cdot \log_{10}\left(\frac{L^2}{\sum_{i=1}^{N}(t^i - \hat{t}^i)}\right) \tag{11}$$

where L denotes the maximum value of a single taxel of the tactile sensor, and, $L = 2$ in this research. PSNR evaluates the quality of the generated image by comparing the errors between the corresponding pixels of two patterns.

2) Structural SIMilarity (SSIM): It is defined by measuring the structural similarity between patterns, based on independent comparisons in terms of intensity, contrast and structures.

$$\begin{aligned}\mu_T &= \frac{1}{N}\sum_{i=1}^{N} t^i \\ \sigma_T &= \left(\frac{1}{N-1}\sum_{i=1}^{N}(t^i - \mu_T)\right)^{\frac{1}{2}} \\ \sigma_{T\hat{T}} &= \frac{1}{N-1}\sum_{i=1}^{N}(t^i - \mu_T)(\hat{t}^i - \mu_{\hat{T}})\end{aligned} \tag{12}$$

where μ_T, σ_T are the mean and variance of tactile patterns, and indicate the intensities and contrasts of the patterns. $\sigma_{T\hat{T}}$ is the covariance between T and $\hat{T}$. The SSIM between T and $\hat{T}$ is defined as follows:

$$\mathrm{SSIM}(T, \hat{T}) = \frac{(2\mu_T\mu_{\hat{T}} + C_1)(2\sigma_{T\hat{T}} + C_2)}{(\mu_T^2 + \mu_{\hat{T}}^2 + C_1)(\sigma_T^2 + \sigma_{\hat{T}}^2 + C_2)} \tag{13}$$

where C_1 and C_2 are constants for avoiding instability (when either $\mu_T^2 + \mu_{\hat{T}}^2$ or $\sigma_T^2 + \sigma_{\hat{T}}^2$ is very close to zero). Typically, $C_1 = 0.01, C_2 = 0.03$.

For the evaluation of the tactile pattern, both PSNR and SSIM are used to reflect the difference between the predicted pattern and the ground truth. PSNR considers the differences in both shape and force distribution, while SSIM focuses primarily on the difference in shape. Higher values of PSNR and SSIM indicate a smaller difference between the predicted and the actual patterns.

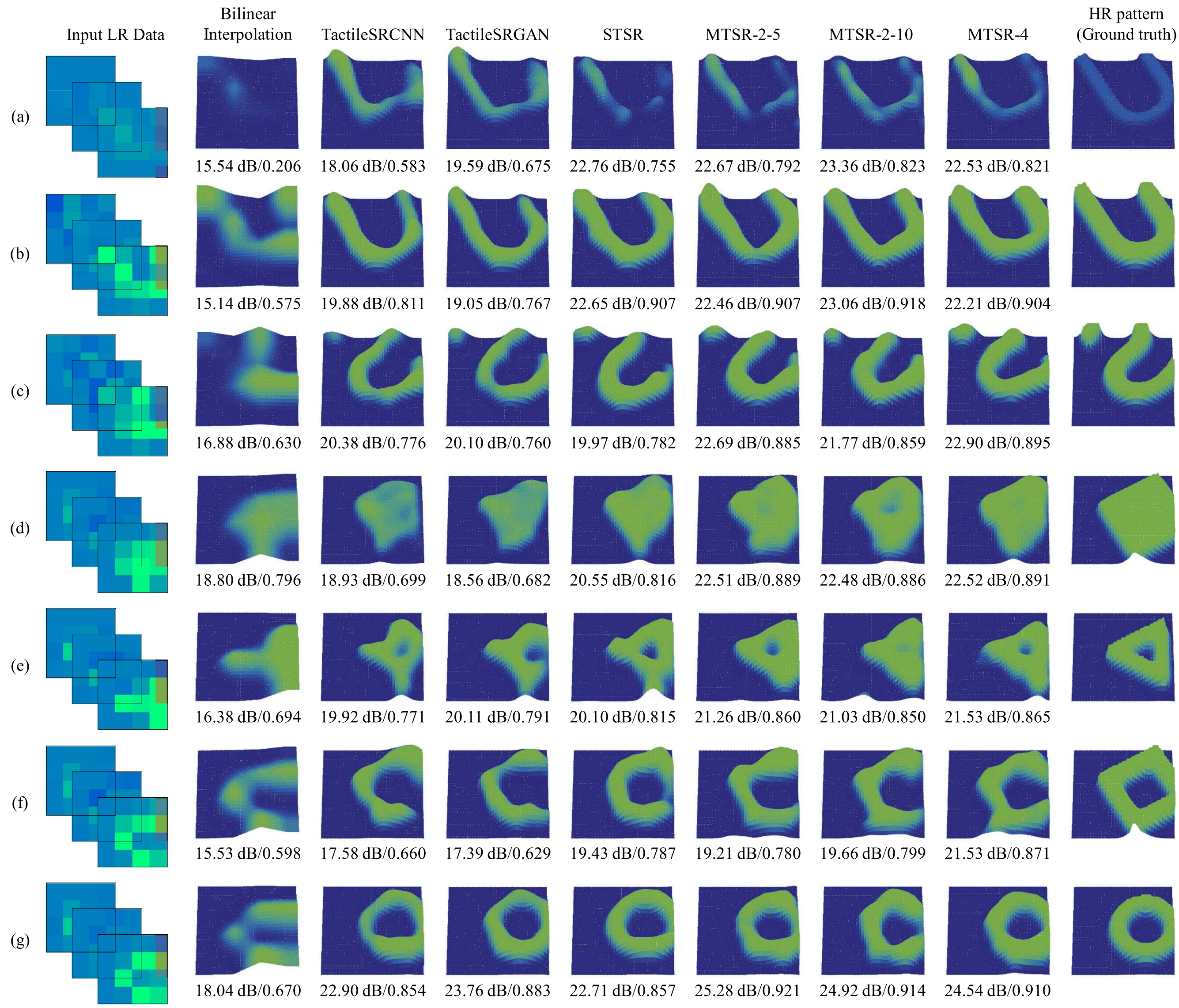

Fig. 9. Experimental results with different tactile pattern SR algorithms. (a $\sim$ c) are the data in the test set, where (a,b) have the same contact pattern, but different contact forces. (d $\sim$ g) are the contact surfaces included in the data set, but the contact pattern is random (not included in the dataset). MTSR-2-5 and MTSR-2-10 represent two-times tapping with 5° and 10° tapping interval, respectively. MTSR-4 means four-times tapping with 5° tapping interval. The input LR data of MTSR shows the LR data of last tapping. The corresponding PSNR and SSIM results are displayed below the figures.

B. Performance Evaluation Scenario I: Cases Based on the Dataset

We compare the proposed scheme with the bilinear interpolation algorithm, TactileSRCNN and TactileSRGAN [20] with a SR scaling factor of 10 (which means a tactile pattern SR from 4×4 to 40×40). Experimental results are shown in Table III and Fig. 9 We can see that the proposed STSR and MTSR outperform all compared schemes in terms of PSNR and SSIM performance.

1) STSR: Comparing the STSR with TactileSRCNN and TactileGAN developed in [20], we can conclude that the presence of pattern and force feature extraction layer allows the proposed model to preserve force features while predicting the shape of the contact pattern, and therefore contributes the most to the performance enhancement.

TABLE III
RESULTS OF DIFFERENT SR ALGORITHMS ON VALIDATION AND TEST SETS, AND THE SR SCALE FACTOR IS 10

Method	Validation set		Test set	
	PSNR	SSIM	PSNR	SSIM
Bilinear	17.31	0.5128	18.10	0.5663
TactileSRCNN	22.17	0.8277	21.10	0.7690
TactileSRGAN	22.05	0.8241	21.54	0.7876
STSR	22.71	0.8373	22.45	0.8170
MTSR-2	24.21	0.9066	23.80	0.8954
MTSR-3	23.72	0.8955	23.73	0.8907
MTSR-4	23.91	0.8980	23.69	0.8934
MTSR-5	23.82	0.8974	24.06	0.9068
MTSR-6	24.02	0.9016	23.93	0.8984
MTSR-7	23.72	0.8981	24.04	0.9004

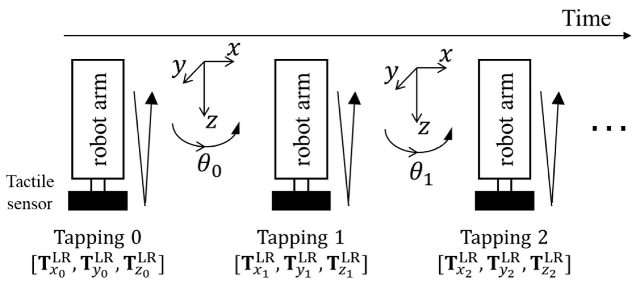

Fig. 10. Trajectory of the tactile sensor in the MTSR. The robot arm slowly descends along the Z-axis until the sensor reaches the object. After completing the first tapping, the robot arm returns to its initial position and then rotates θ_0 for the next tapping.

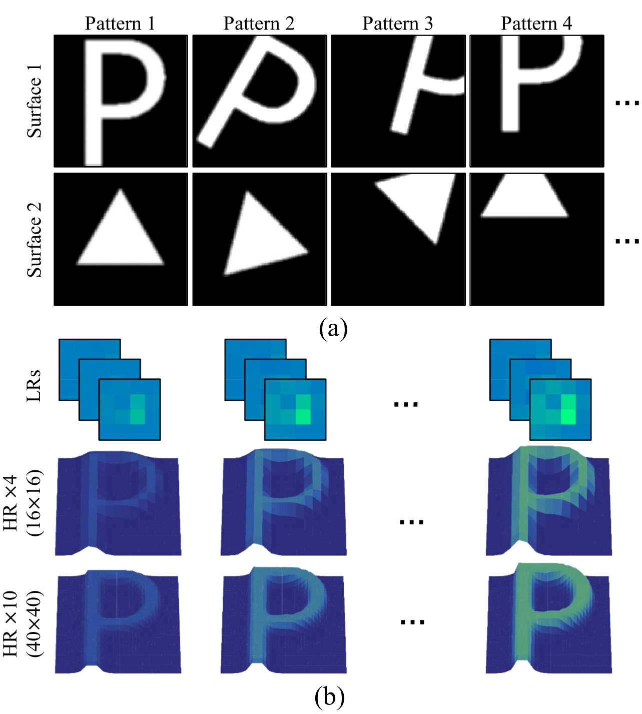

Fig. 11. Exemplar of the new dataset. (a) Depth of contact patterns in the dataset. The tactile sensor makes contact with the surface in different poses, each pose corresponding to a unique contact pattern. A total of 648 contact patterns, collected from 18 contact surfaces, are included in the dataset. (b) The depth remains constant throughout a tapping process, and LR sequences are collected to generate HR data using the proposed tactile PSF.

In addition, we discover from Table IV that the proposed scheme can achieve satisfactory performance with respect to different scaling factors, which indicates that the proposed SR model can effectively recover the primary information such as the contours of the contact surfaces. We should admit that the proposed scheme struggles to predict the more intricate texture information due to the LR inputs of taxel-based sensors. Fortunately, a fine texture reconstruction is unnecessary in many robotic applications (e.g. grasping), where the contour of the contact surface and to-be-applied force are important to task success.

2) MTSR: The proposed STSR approach demonstrates promising performance for the SR of contact surfaces in the dataset. However, there are instances, such as in Fig. 9(f) and (g), where the input LR data are nearly identical, resulting in difficulties to distinguish the corresponding contact patterns accurately. To address this challenge, we propose the MTSR strategy, which improve the prediction accuracy by collecting additional data through multiple samplings of the contact surface, as described in Fig. 10.

TABLE IV
RESULTS OF STSR ON VALIDATION AND TEST SETS WITH DIFFERENT SR SCALE FACTORS

Method	Size	Validation set PSNR	Validation set SSIM	Test set PSNR	Test set SSIM
×4	16 × 16	23.12	0.8507	22.69	0.8297
×6	24 × 24	22.98	0.8475	22.84	0.8326
×8	32 × 32	22.54	0.8345	22.12	0.8108
×10	40 × 40	22.71	0.8373	22.45	0.8170
×20	80 × 80	23.15	0.8481	22.56	0.8219

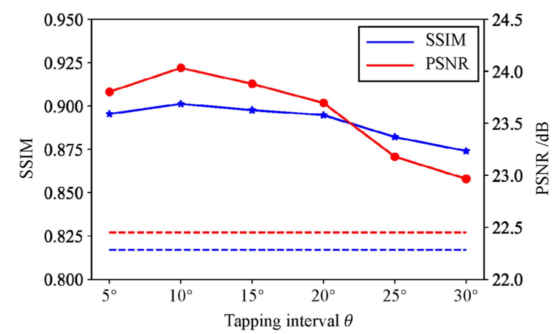

Fig. 12. PSNR and SSIM results of MTSR ($K = 2$) with respect to different rotation angles (scaling factor $p = 10$, denoting a resulting tactile pattern resolution of 40 × 40). Two dashed lines represent the corresponding results of STSR.

A natural question to ask is what is the best rotation angle between two tapping instance in the MTSR scheme? We illustrate the PSNR and SSIM results of MTSR when $K = 2$ (denoting the number of tapping actions) and SR scaling factor $p = 10$ with respect to rotation angles of $5°, 10°, 15°, 20°, 25°$, and $30°$. The experimental results are shown in Fig. 12. We can observe a slightly increase followed by gradual declines in the performance as the increase of the rotation angle θ. According to Fig. 12, the proposed SR model achieves the best performance when $\theta = 10°$ in the test set (but not necessarily in real-world cases). Intuitively, a suitable small interval between two tapping instances allows the SR model to extract useful information effectively. Without loss of generality, we set $\theta = 5°$ in the following experiments.

Fig. 13 presents the PSNR and SSIM performance of the proposed scheme with respect to different numbers of tapping instances. We can observe that there is a significant performance enhancement in MTSR when $K = 2$ compared with the STSR. However, the improvement becomes steady when $K > 2$. This indicates that two tappings are sufficient to predict the shape of contact surfaces in the dataset effectively. This observation will not hold for real-world cases, which will be demonstrated in the next section.

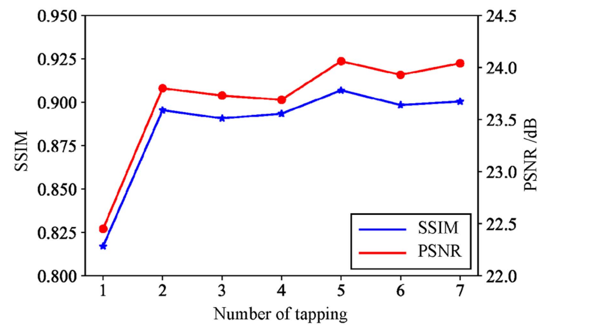

Fig. 13. PSNR and SSIM performance of the proposed SR scheme in the test set in terms of number of tapping instants.

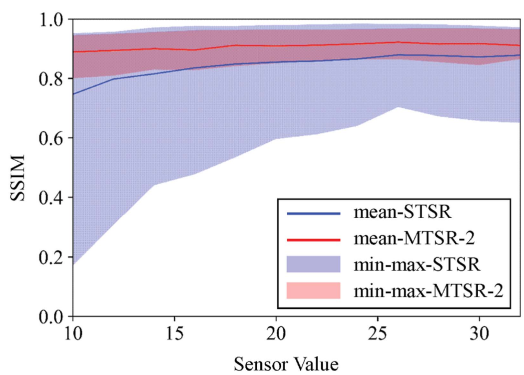

Fig. 14. Illustration on the variation of SSIM performance of the proposed scheme under different contact conditions.

With small contact force, the sensor and the contact surface are in a state of fresh contact during the tapping process, which results in a significant impact of sensor noise on the model performance. As shown in Fig. 14, when the contact force is small, the predicted shape of the SR model fluctuates greatly due to the influence of sensor noise and other factors in the case of STSR. However, the MTSR approach can effectively remove the noise interference by leveraging the information from previous tappings, enabling the proposed SR model to maintain a satisfactory performance even for the small contact force scenario.

C. Performance Evaluation Scenario II: Real-World Cases

In this section, we demonstrate the experimental results of the proposed SR scheme in real-world cases where all contact surfaces are not included in the dataset.

1) Force Recovery: One key contribution of the proposed SR scheme lies in the guarantee of accurate force recovery while contact pattern shape reconstruction. This outcome strongly outperforms the TactileSRCNN and TactileSRGAN algorithms developed in [20], as shown in Fig. 15. In [20], the dataset only include LR-HR data pairs at the maximum contact force as the sensor touches the object. In this paper, we employ the PSF method to generate a series of LR-HR pairs from the initial contact to the maximum contact force moment. We also strategically

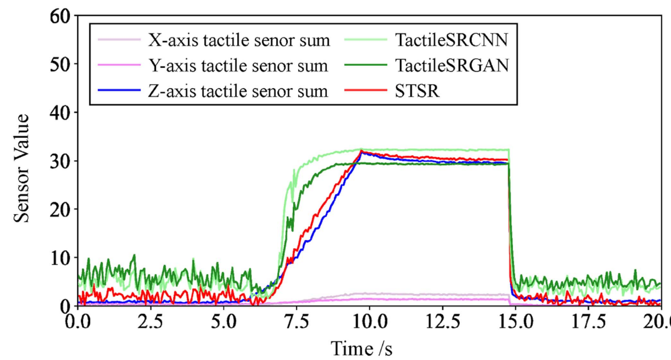

Fig. 15. Illustration of force recovery performance. At t=7.5 s, the sensor starts the tapping action and moves toward the contact object. At t=10 s, the sensor reaches the set threshold and remains in contact for 5 seconds before lifting vertically away from the object.

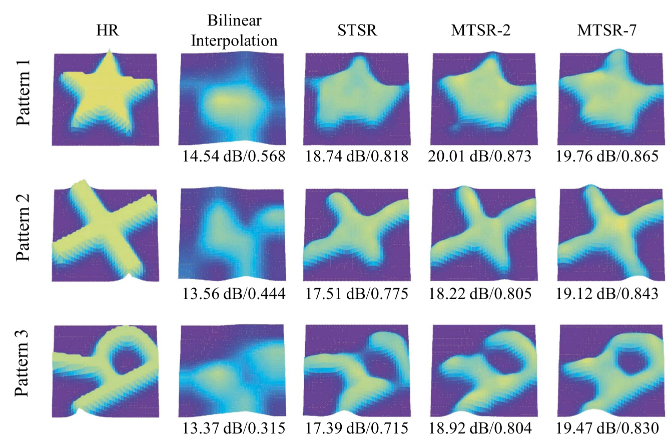

Fig. 16. Experimental result of contact surface not in dataset. Below the pictures are the corresponding PSNR and SSIM results.

design the force feature extraction layer in the proposed scheme to enhance the performance.

In this study, we did not directly predict the HR force map of the sensor surface. Rather, since the ground truth generated by tPSF is the Z-axis deformation map of the sensor surface, the SR models predict the deformation data of the sensor under different contact forces. The deformation map is usually positively correlated with the applied force, with larger deformation typically indicating larger force.

2) Shape Recovery: A key task of the proposed SR model is to accurately reconstruct the shape of contact patterns using LR data. Our experiments reveal that the proposed model can effectively recover the shape of contact surfaces that are similar to those in the dataset or that have clear and distinguishable tactile features. Unfortunately, the performance of the proposed scheme degrades when the contact surface is beyond the generalization ability of the proposed scheme. In Fig. 16, we present three contact surfaces out of the dataset. The tactile features of *pattern2* are relatively simple, while *pattern3* resembles a contact surface present in the dataset. Hence, the proposed scheme achieves a better shape recovery of these two contact patterns compared with that of *pattern1*, where the limited input data obtained from a single tapping leads to an unsatisfactory prediction of the contact shape. As the number of taps increases, the prediction result becomes more accurate, demonstrating that multiple tapping instances can provide more meaningful information on the contact surface and thereby improve the generalization performance of the proposed model.

In conclusion, our experimental results demonstrate the robust generalization capabilities of the tactileSR model across diverse scenarios. When the model encounters scenarios of familiar contact surfaces but unknown poses, it consistently exhibits high accuracy in HR data prediction, as presented in Section VI-B. This robustness is vital for practical applications, given the impracticality of training on all conceivable poses. Furthermore, for entirely unfamiliar contact surfaces, our model maintains a satisfactory performance, especially when these surfaces bear resemblance to those in the training set, as shown in Section VI-C. Nonetheless, it is important to acknowledge that the model's proficiency in accurately predicting interactions with complex and unfamiliar surfaces remains limited. To overcome this limitation, we have introduced the MTSR approach, which enhances the tactileSR model's generalization by incorporating multiple tapping inputs. This method shows promise in significantly improving the model's adaptability to complex and unfamiliar surfaces.

VII. Conclusion

In this paper, we presented a novel tactile PSF method that can be utilized to efficiently simulate the deformation of the sensor surface, which helped to generate HR tactile patterns with scalable resolutions, and built up a new dataset with LR-HR data pairs for tactile SR. We further proposed a novel tactile pattern SR model by incorporating both shape and force feature extraction layers into the feature extraction module. The input layer of our SR model can be adjusted to accommodate multi-tapping scenarios. We evaluated the proposed SR scheme within the dataset as well as real-world cases, and obtained promising results compared with traditional interpolation methods and the state-of-the-art tactile SR algorithms (i.e. tactileSRCNN and tactileSRGAN [20]).

In the MTSR scheme, we only considered an uniform rotation angle θ for all tapping instances and all contact surfaces. In fact, it is advisable to rotate from an optimal angle θ_{best} to acquire more valuable information with fewer tapping instances. In addition, we may investigate how to use the prior information and LR data from the first tapping to actively determine the next tapping pose, so as to improve the accuracy and efficiency of shape reconstruction.

However, we must acknowledge a limitation in this work, particular in its application to non-planar contact situations. The proposed tactile PSF method primarily focuses on planar objects, leveraging a single PSF to simulate the deformation distribution. This model may not accurately represent the complex deformation distributions of non-planar objects like spheres or cylinders. In our future work, we approximate non-planar objects as consisting of multiple planar of different heights, each of which we can use a individual PSF to describe. The number of PSFs is determined by the geometry of the surface, which can be described by the depth image. This advancement will enable a more accurate characterization of contact forces in diverse and non-planar tactile interactions, thus broadening the applicability of our research in real-world scenarios.

In addition, investigating the correlation between the PSF, depth image, and shear deformation, followed by the development of shear deformation tactile pattern SR model is an interesting topic for future work.

Acknowledgment

The authors gratefully acknowledge the assistance of ChatGPT for initial linguistic refinement during the preliminary drafting phase of this manuscript. It is, however, emphasized that the substantive scientific contributions, data interpretation, and the critical conclusions drawn herein were exclusively the work of the authors.

References

[1] Y. She, S. Wang, S. Dong, N. Sunil, A. Rodriguez, and E. Adelson, "Cable manipulation with a tactile-reactive gripper," *Int. J. Robot. Res.*, vol. 40, no. 12/14, pp. 1385–1401, 2021.

[2] Y. Gao, D. Wu, and L. Zhou, "How to improve immersive experience?," *IEEE Trans. Multimedia*, early access, Aug. 17, 2022, doi: 10.1109/TMM.2022.3199666.

[3] R. Calandra et al., "The feeling of success: Does touch sensing help predict grasp outcomes?," in *Proc. Conf. Robot Learn.*, 2017, pp. 314–323.

[4] Y. Li, J.-Y. Zhu, R. Tedrake, and A. Torralba, "Connecting touch and vision via cross-modal prediction," in *Proc. IEEE/CVF Conf. Comput. Vis. Pattern Recognit.*, 2019, pp. 10 609–10 618.

[5] L. Zou, C. Ge, Z. J. Wang, E. Cretu, and X. Li, "Novel tactile sensor technology and smart tactile sensing systems: A review," *Sensors*, vol. 17, no. 11, 2017, Art. no. 2653.

[6] W. Yuan, S. Dong, and E. H. Adelson, "GelSight: High-resolution robot tactile sensors for estimating geometry and force," *Sensors*, vol. 17, no. 12, 2017, Art. no. 2762.

[7] E. Donlon, S. Dong, M. Liu, J. Li, E. Adelson, and A. Rodriguez, "GelSlim: A high-resolution, compact, robust, and calibrated tactile-sensing finger," in *Proc. IEEE/RSJ Int. Conf. Intell. Robots Syst.*, 2018, pp. 1927–1934.

[8] B. Ward-Cherrier et al., "The tactip family: Soft optical tactile sensors with 3D-printed biomimetic morphologies," *Soft Robot.*, vol. 5, no. 2, pp. 216–227, 2018.

[9] H. Sun, K. J. Kuchenbecker, and G. Martius, "A soft thumb-sized vision-based sensor with accurate all-round force perception," *Nature Mach. Intell.*, vol. 4, no. 2, pp. 135–145, 2022.

[10] N. F. Lepora, "Soft biomimetic optical tactile sensing with the TacTip: A review," *IEEE Sensors J.*, vol. 21, no. 19, pp. 21 131–21 143, Oct. 2021.

[11] Q. K. Luu, N. H. Nguyen, and V. A. Ho, "Simulation, learning, and application of vision-based tactile sensing at large scale," *IEEE Trans. Robot.*, vol. 39, no. 3, pp. 2003–2019, Jun. 2023.

[12] Z. Kappassov, J.-A. Corrales, and V. Perdereau, "Tactile sensing in dexterous robot hands," *Robot. Auton. Syst.*, vol. 74, pp. 195–220, 2015.

[13] S. Sundaram, P. Kellnhofer, Y. Li, J.-Y. Zhu, A. Torralba, and W. Matusik, "Learning the signatures of the human grasp using a scalable tactile glove," *Nature*, vol. 569, no. 7758, pp. 698–702, 2019.

[14] C. Becker et al., "A new dimension for magnetosensitive e-skins: Active matrix integrated micro-origami sensor arrays," *Nature Commun.*, vol. 13, no. 1, 2022, Art. no. 2121.

[15] P. A. Schmidt, E. Maël, and R. P. Würtz, "A sensor for dynamic tactile information with applications in human–robot interaction and object exploration," *Robot. Auton. Syst.*, vol. 54, no. 12, pp. 1005–1014, 2006.

[16] A. Drimus, G. Kootstra, A. Bilberg, and D. Kragic, "Design of a flexible tactile sensor for classification of rigid and deformable objects," *Robot. Auton. Syst.*, vol. 62, no. 1, pp. 3–15, 2014.

[17] H.-K. Lee, J. Chung, S.-I. Chang, and E. Yoon, "Normal and shear force measurement using a flexible polymer tactile sensor with embedded multiple capacitors," *J. Microelectromech. Syst.*, vol. 17, no. 4, pp. 934–942, 2008.

[18] A. Charalambides and S. Bergbreiter, "A novel all-elastomer MEMS tactile sensor for high dynamic range shear and normal force sensing," *J. Micromechanics Microengineering*, vol. 25, no. 9, 2015, Art. no. 095009.

[19] R. S. Dahiya, G. Metta, M. Valle, and G. Sandini, "Tactile sensing–from humans to humanoids," *IEEE Trans. Robot.*, vol. 26, no. 1, pp. 1–20, Feb. 2010.

[20] B. Wu, Q. Liu, and Q. Zhang, "Tactile pattern super resolution with taxel-based sensors," in *Proc. IEEE/RSJ Int. Conf. Intell. Robots Syst.*, 2022, pp. 3644–3650.

[21] C. Dong, C. C. Loy, K. He, and X. Tang, "Learning a deep convolutional network for image super-resolution," in *Proc. Eur. Conf. Comput. Vis.*, 2014, pp. 184–199.

[22] C. Ledig et al., "Photo-realistic single image super-resolution using a generative adversarial network," in *Proc. IEEE Conf. Comput. Vis. Pattern Recognit.*, 2017, pp. 4681–4690.

[23] T. P. Tomo et al., "Design and characterization of a three-axis hall effect-based soft skin sensor," *Sensors*, vol. 16, no. 4, 2016, Art. no. 491.

[24] W. Yang, X. Zhang, Y. Tian, W. Wang, J.-H. Xue, and Q. Liao, "Deep learning for single image super-resolution: A brief review," *IEEE Trans. Multimedia*, vol. 21, no. 12, pp. 3106–3121, Dec. 2019.

[25] A. Kappeler, S. Yoo, Q. Dai, and A. K. Katsaggelos, "Video super-resolution with convolutional neural networks," *IEEE Trans. Comput. Imag.*, vol. 2, no. 2, pp. 109–122, Jun. 2016.

[26] N. F. Lepora, U. Martinez-Hernandez, M. Evans, L. Natale, G. Metta, and T. J. Prescott, "Tactile superresolution and biomimetic hyperacuity," *IEEE Trans. Robot.*, vol. 31, no. 3, pp. 605–618, Jun. 2015.

[27] N. F. Lepora and B. Ward-Cherrier, "Superresolution with an optical tactile sensor," in *Proc. IEEE/RSJ Int. Conf. Intell. Robots Syst.*, 2015, pp. 2686–2691.

[28] P. Piacenza, S. Sherman, and M. Ciocarlie, "Data-driven super-resolution on a tactile dome," *IEEE Robot. Automat. Lett.*, vol. 3, no. 3, pp. 1434–1441, Jul. 2018.

[29] H. Sun and G. Martius, "Guiding the design of superresolution tactile skins with taxel value isolines theory," *Sci. Robot.*, vol. 7, no. 63, 2022, Art. no. eabm0608.

[30] M. Kim, H. Choi, K.-J. Cho, and S. Jo, "Single to multi: Data-driven high resolution calibration method for piezoresistive sensor array," *IEEE Robot. Automat. Lett.*, vol. 6, no. 3, pp. 4970–4977, Jul. 2021.

[31] T. Hellebrekers, N. Chang, K. Chin, M. J. Ford, O. Kroemer, and C. Majidi, "Soft magnetic tactile skin for continuous force and location estimation using neural networks," *IEEE Robot. Automat. Lett.*, vol. 5, no. 3, pp. 3892–3898, Jul. 2020.

[32] Y. Yan et al., "Soft magnetic skin for super-resolution tactile sensing with force self-decoupling," *Sci. Robot.*, vol. 6, no. 51, 2021, Art. no. eabc8801.

[33] Y. Yan, Y. Shen, C. Song, and J. Pan, "Tactile super-resolution model for soft magnetic skin," *IEEE Robot. Automat. Lett.*, vol. 7, no. 2, pp. 2589–2596, Apr. 2022.

[34] H. Lee, K. Park, J. Kim, and K. J. Kuchenbecker, "Internal array electrodes improve the spatial resolution of soft tactile sensors based on electrical resistance tomography," in *Proc. Int. Conf. Robot. Automat.*, 2019, pp. 5411–5417.

[35] Z. Husain, N. A. Madjid, and P. Liatsis, "Tactile sensing using machine learning-driven electrical impedance tomography," *IEEE Sensors J.*, vol. 21, no. 10, pp. 11 628–11 642, May 2021.

[36] H. Park, K. Park, S. Mo, and J. Kim, "Deep neural network based electrical impedance tomographic sensing methodology for large-area robotic tactile sensing," *IEEE Trans. Robot.*, vol. 37, no. 5, pp. 1570–1583, Oct. 2021.

[37] K. Park, H. Yuk, M. Yang, J. Cho, H. Lee, and J. Kim, "A biomimetic elastomeric robot skin using electrical impedance and acoustic tomography for tactile sensing," *Sci. Robot.*, vol. 7, no. 67, 2022, Art. no. eabm7187.

[38] C. Hui, S. Hanqiu, and J. Xiaogang, "Interactive haptic deformation of dynamic soft objects," in *Proc. ACM Int. Conf. Virtual Reality Continuum Appl.*, 2006, pp. 255–261.

[39] A. Habib, I. Ranatunga, K. Shook, and D. O. Popa, "SkinSim: A simulation environment for multimodal robot skin," in *Proc. IEEE Int. Conf. Automat. Sci. Eng.*, 2014, pp. 1226–1231.

[40] D. Ma, E. Donlon, S. Dong, and A. Rodriguez, "Dense tactile force estimation using GelSlim and inverse fem," in *Proc. Int. Conf. Robot. Automat.*, 2019, pp. 5418–5424.

[41] C. Sferrazza, T. Bi, and R. D'Andrea, "Learning the sense of touch in simulation: A sim-to-real strategy for vision-based tactile sensing," in *Proc. IEEE/RSJ Int. Conf. Intell. Robots Syst.*, 2020, pp. 4389–4396.

[42] C. Sferrazza, A. Wahlsten, C. Trueeb, and R. D'Andrea, "Ground truth force distribution for learning-based tactile sensing: A finite element approach," *IEEE Access*, vol. 7, pp. 173438–173449, 2019.

[43] Y. Wang, W. Huang, B. Fang, F. Sun, and C. Li, "Elastic tactile simulation towards tactile-visual perception," in *Proc. 29th ACM Int. Conf. Multimedia*, 2021, pp. 2690–2698.

[44] Z. Chen, S. Zhang, S. Luo, F. Sun, and B. Fang, "Tacchi: A pluggable and low computational cost elastomer deformation simulator for optical tactile sensors," *IEEE Robot. Automat. Lett.*, vol. 8, no. 3, pp. 1239–1246, Mar. 2023.

[45] Y. Narang, B. Sundaralingam, M. Macklin, A. Mousavian, and D. Fox, "Sim-to-real for robotic tactile sensing via physics-based simulation and learned latent projections," in *Proc. IEEE Int. Conf. Robot. Automat.*, 2021, pp. 6444–6451.

[46] S. Wang, M. Lambeta, P.-W. Chou, and R. Calandra, "TACTO: A fast, flexible, and open-source simulator for high-resolution vision-based tactile sensors," *IEEE Robot. Automat. Lett.*, vol. 7, no. 2, pp. 3930–3937, Apr. 2022.

[47] Z. Si and W. Yuan, "Taxim: An example-based simulation model for gelsight tactile sensors," *IEEE Robot. Automat. Lett.*, vol. 7, no. 2, pp. 2361–2368, Apr. 2022.

[48] Z. Pezzementi, E. Jantho, L. Estrade, and G. D. Hager, "Characterization and simulation of tactile sensors," in *Proc. IEEE Haptics Symp.*, 2010, pp. 199–205.

[49] Z. Kappassov, J.-A. Corrales-Ramon, and V. Perdereau, "Simulation of tactile sensing arrays for physical interaction tasks," in *Proc. IEEE/ASME Int. Conf. Adv. Intell. Mechatron.*, 2020, pp. 196–201.

[50] Z. Pezzementi, C. Reyda, and G. D. Hager, "Object mapping, recognition, and localization from tactile geometry," in *Proc. IEEE Int. Conf. Robot. Automat.*, 2011, pp. 5942–5948.

[51] Z. Pezzementi, E. Plaku, C. Reyda, and G. D. Hager, "Tactile-object recognition from appearance information," *IEEE Trans. Robot.*, vol. 27, no. 3, pp. 473–487, Jun. 2011.

[52] J. Li, F. Fang, K. Mei, and G. Zhang, "Multi-scale residual network for image super-resolution," in *Proc. Eur. Conf. Comput. Vis.*, 2018, pp. 517-532.

[53] K. He, X. Zhang, S. Ren, and J. Sun, "Delving deep into rectifiers: Surpassing human-level performance on ImageNet classification," in *Proc. IEEE Int. Conf. Comput. Vis.*, 2015, pp. 1026–1034.

[54] Z. Wang, J. Chen, and S. C. H. Hoi, "Deep learning for image super-resolution: A survey," *IEEE Trans. Pattern Anal. Mach. Intell.*, vol. 43, no. 10, pp. 3365–3387, Oct. 2021.

Bing Wu received the B.S. degrees in mechanical engineering in 2021 from the Dalian University of Technology, Dalian, China, where he is currently working toward the M.S. degree. His research interests include tactile perception and robotic.

Qian Liu received the Ph.D. degree from the State University of New York at Buffalo (SUNY-Buffalo), Amherst, NY, USA, in 2013. She is currently a Professor with the Department of Computer Science and Technology, Dalian University of Technology, Dalian, China. She was a Postdoctoral Fellow with the Ubiquitous Multimedia Laboratory, SUNY-Buffalo from 2013 to 2015. She was an Alexander von Humboldt Fellow with the Chair of Media Technology and the Chair of Communication Networks, Technical University of Munich, Munich, Germany, from 2016 to 2017. Her current research interests include haptic signal processing and communications, wireless multimedia communications, and haptic human-computer interaction. She provides services to the IEEE Haptic Codec Task Group as a secretary for standardizing haptic codecs in the Tactile Internet. She was also the Technical Program Chair of 2017 IEEE HAVE'17, HAVE'18, AsiaHaptics 2020, and AsiaHaptics 2022.